An atomistic investigation of the effect of strain on frictional properties of suspended graphene

Qingshun Bai,[1] Xin He,[1] Jinxuan Bai,[1] and Zhen Tong[2]
[1]*School of Mechanical and Electrical Engineering, Harbin Institute of Technology, Harbin 150001, People's Republic of China*
[2]*Centre for precision technologies, University of Huddersfield, Huddersfield, HD1 3DH, UK*

(Received 10 December 2015; accepted 28 April 2016; published online 9 May 2016)

We performed molecular dynamics (MD) simulations of a diamond probe scanned on a suspended graphene to reveal the effect of strain on the frictional properties of suspended graphene. The graphene was subjected to some certain strain along the scanning direction. We compared the friction coefficient obtained from different normal loads and strain. The results show that the friction coefficient can be decreased about one order of magnitude with the increase of the strain. And that can be a result of the decreased asymmetry of the contact region which is caused by strain. The synthetic effect of potential energy and the fluctuation of contact region were found to be the main reason accounting for the fluctuation of the friction force. The strain can reduce the fluctuation of the contact region and improve the stability of friction.
[http://dx.doi.org/10.1063/1.4949521]

I. INTRODUCTION

The development of the macro- or nanoelectromechanical systems (M/NEMS) highlights the need to develop new lubricant for nanosale structures. Because the extremely high relative surface area at micro- or nanoscales renders heavy adhesion, friction, and wear for the movable parts. Graphene, a two-dimensional material consisting of sp^2-hybridized carbon atoms, has been attracting great interest for its outstanding electronic,[1] thermal[2] and mechanical[3] properties. Meanwhile, the superlubricity of graphite has been achieved at both nano- and microscales,[4–6] and it may be an promising solid lubricant for M/NEMS.[7,8] Therefore, an in-depth understand of the tribological properties of graphene is required for its engineering implementation in future M/NEMS.[9–11]

The thickness dependence of friction, friction increased as the layer of graphene decreased, has been observed in many studies. This effect is attributed to the 'puckers' formed in front of the scanning tip, which can be called puckering effect.[7,12] This dependence could be different for various materials or morphologies of the substrate because of the variation of the adhesive force between substrate and graphene.[12–14] The adhesion between atomic force microscope (AFM) probe and graphene can also affect the friction force and lead to the emergence of an effectively negative friction coefficient.[15] Meanwhile, electro-phonon coupling and shear deformations were also brought to explain the energy dissipation mechanism during the friction process.[16–19] A recent study revealed that the friction force of chemically modified graphene is mainly governed by the out of plane bending stiffness.[20,21] Therefore, due to low bending rigidity, the friction of strained supported few layer graphene can be decreased significantly by the radial strain, since the strain could smooth out the graphene and decrease the contact between graphene and substrate.[22] Based on the research of the supported and suspended graphene, a great difference of the friction properties between these two conditions can be observed.[23] For the suspended graphene, the elastic deformation, dominated by out-of-plane stiffness, is the major factor contributing to friction.[24–26]

To our knowledge, little work about the effect of strain on the friction of suspended graphene has been reported until now. In this paper, molecular dynamics (MD) simulation was applied to study the sliding interaction between the diamond AFM probe and the strained suspended graphene

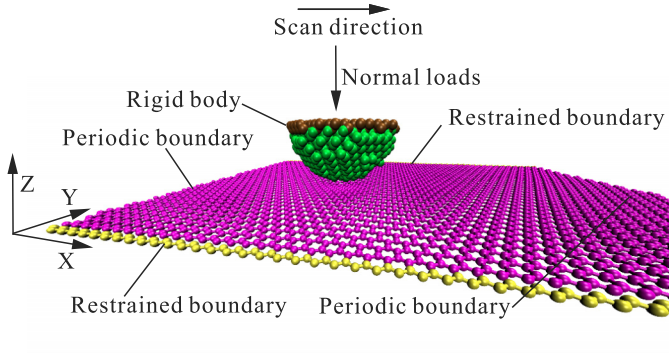

FIG. 1. Schematic of the simulation system.

to explore the effect of strain on atomic-level frictional properties. We changed the strain and the vertical loads applied on the tip to examine the variation of the friction force. Through the analysis of the contact region, we revealed that the mechanism of the dramatic decrease of the friction coefficient with the increase of strain is related closely to the asymmetry of the contact region. We also studied the fluctuation of the friction force. The results suggest that it is influenced by both potential energy[24] and the fluctuation of the contact region.

II. MODELING AND CONDITIONS FOR THE CONTACT SIMULATION

As shown in Fig. 1, the model system for contact simulation composes a monolayer graphene and an AFM probe. The probe is modeled by a hemispheric diamond tip with radius of 1.5 nm. The initial size of the graphene sheet was 12nm×8nm. The uppermost atomic layers of the probe were set to rigidly scanned against the suspended graphene at a prescribed velocity of 10 m/s along X-direction, in which process, a constant vertical load was applied on the rigid layers. We first relax the graphene layer to achieve minimal energy. Subsequently, the graphene was strained parallel to the tip scanning direction (X-direction) through deforming the length of simulation box at a constant engineering strain rate of 0.001/ps. This strain, which can be called pre-strain, will be hold during the following simulations. Then the system was equilibrated for 100 ps under a Nosé-Hoover barostat and thermostat method (NPT) to keep the Y-stress of the system to be about zero. Next, a normal load was applied on diamond tip. The entire system was further equilibrated for 20ps and followed friction process started. The loading and friction simulation were performed under Langevin thermostat[27] with a damping constant of γ=3.32·10^{-12} Kg/s.[25] The temperature in all of the simulations was controlled at 10K. To avoid the boundary effects, periodic boundary conditions (PBC) were applied in X-direction and the atoms along Y-boundaries were fixed to support the sample. The interaction between the graphene layer and the tip was calculated by the Lennard-Jones potential with ε=0.028 eV, σ=3.4 Å and a cutoff radius of 10.2 Å. The AIREBO[28] potential was used to simulate the C-C atomic interactions within graphene and diamond tip. All simulations were run for a duration of 600 ps with a constant time step of 1 fs. Thereafter, the total interaction in X-direction between graphene layer and diamond tip was averaged over every 500 MD time-steps. These mean values could be averaged again over the last five periods of the friction force, and the final interaction value was reckoned as the nominal friction force.

III. RESULTS AND DISCUSSION

A. Effect of the strain on the friction coefficient

Fig. 2 shows the relationship between the friction coefficient μ and the pre-strain υ. For the non-pre-strained graphene, the friction coefficient decreased from 0.067 to 0.045 when the loads increased from 4 nN to 16 nN. The results present a good agreement with the experimental values

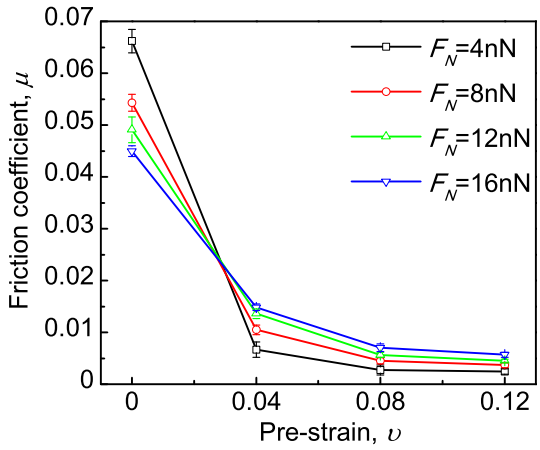

FIG. 2. Relationship between friction coefficient and pre-strain.

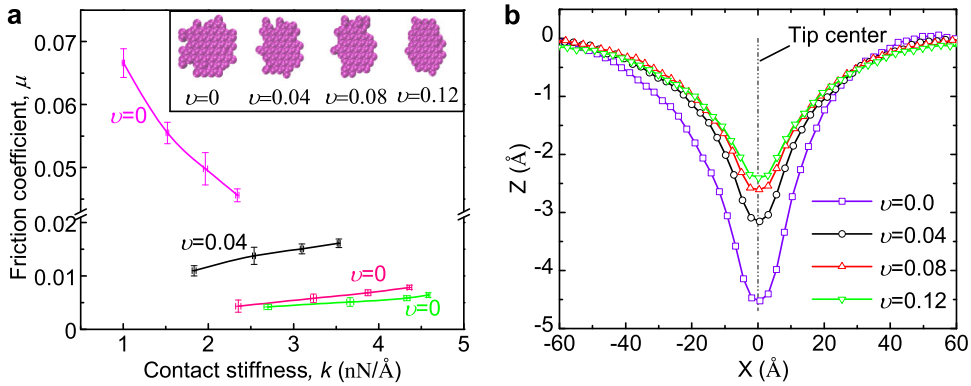

FIG. 3. a, Relationship between μ abd k. The values of k from left to right for each line was obtained from different normal loads of 4 nN, 8 nN, 12 nN and 16 nN respectively. Thus, the relationship between k and F_N is nonlinear. The inset is the top-view of the contact region under different pre-strain. b, Two-dimensional profiles of the out-of-plane deflection of graphene samples with different pre-strain under a normal loads of 12nN. Data points represent the graphene atoms.

reported in Ref. 23 (from 0.080 to 0.0270) and Ref. 29 (μ=0.03). It is found that, under all the tested normal loads, μ decreased with the increase of pre-strain. The descending rate of the friction coefficient slowed down gradually and finally reached a stable value. This trend is similar to the strained supported graphene.[22] When the pre-strain reached 0.12, the friction coefficient can be decreased by about one order of magnitude.

It has been reported that the friction properties of non-strained suspended graphene are mainly affected by elastic deformation energy and thus μ is approximately proportional to the reciprocal of contact stiffness $k=F_N/\delta$,[25] whereF_N is the vertical load applied on diamond tip and δ is the deflection of the graphene layer. As shown in Fig. 3(a), the relationship between k and F_N is nonlinear which is consistent with the experiment.[3] For the non-pre-strained model (υ=0), μ decreased with the increase of k. But for the pre-strained models, μ increased linearly with the increase of k which is not corresponding to the theory of Ref. 25. Meanwhile, $1/k$ decreased by up to 51% during the pre-strain increased from 0 to 0.12, so it would be less likely to result in a sharp decrease in friction coefficient μ. All of those above show that the friction behavior of the pre-strained graphene is no longer can be considered to be affected by the amount of the elastic deformation energy mainly.

The friction between a suspended graphene and a tip has been considered in terms of the effect of the adhesion and the out-of-plane deformation.[26] The contact region between a tip and graphene sheet that is suspended on circular holes should be a spherical crown. In this work, the pre-strain can increase the anisotropy of the graphene sheet, so the shape of the contact region would became

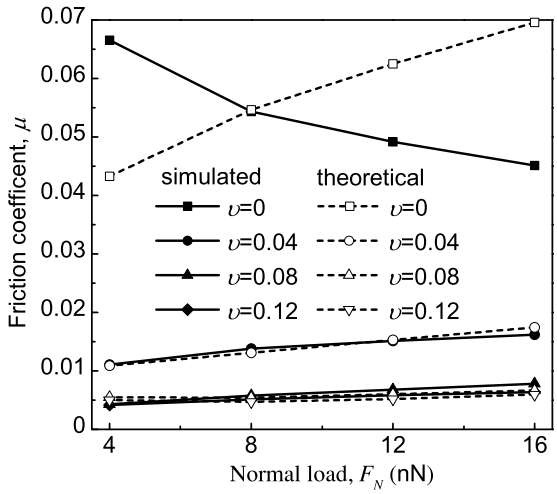

FIG. 4. The simulation and theoretical friction coefficient under various loads (solid curves for simulated μ and dotted curves for theoretical μ).

ellipsoidal gradually as the pre-strain increased (inset in Fig. 3(a)), and thus the simplified model for non-strained graphene[26] is no longer suitable for pre-strained graphene.

According to the friction law at nanoscale,[30] the number of the contact atoms in contact region was taken to charicterize the real contact area A_{real}. Considering the average surface area per atom (A_{at}) will be changed by pre-strain, it can been caculated by $A_{at} = (1 + \upsilon) A_{at,0}$, where $A_{at,0}$ is the initial average surface area per graphene atom when υ=0. Thus the theoretical real contact areal A_{real} can be given as:

$$A_{real} = (1 + \upsilon) N_{at,\upsilon} A_{at,0} \tag{1}$$

Where $N_{at,\upsilon}$ is the number of the contact graphene atoms subjected to a tensile strain of υ. A cutoff distance of 3.4 Å was chosen to determine the two types of atoms were contact or not. Now, the adhesive force $F_{f,vdw}$ can be calculated by:

$$F_{f,vdw} = (1 + \upsilon) \tau N_{at,\upsilon} A_{at,0} \tag{2}$$

Where τ is the shear strength of the graphene, and the value of τ=8 MPa used in this work was derived from Ref. 31. Because the contribution of deformation to friction is directly proportion to deformation energy, $F_{f,p} \sim \frac{F_N^2}{2k}$.[25] Finally, based on comprehensive consideration of adhesive and deformation effect, the friction coefficient can be given as:

$$\mu = \frac{(1 + \varepsilon) \upsilon N_{at,\upsilon} A_{at,0}}{F_N} + \lambda \frac{F_N}{k} \tag{3}$$

where λ is a dimensionless coefficient. The first item at the right side of the equation represents the adhesive effect and the second represents the deformation effect, and they can be denoted as μ_{vdw} and μ_d respectively. The contrast curves of the simulated and theoretical friction coefficient are shown in Fig. 4. They matched very well when the graphene is pre-strained, but a large difference can be found under none-strained situation.

When pre-strain varied from 0 to 0.12, the number of contact atoms only decreased 25%. This small change also cannot cause the sharp decrease of the friction coefficient. In fact, as shown in Fig. 3(b), the out-of-plane deformation is mainly symmetric. Most of the interaction between the graphene and diamond tip can be offset and only the asymmetry of the contact region could oppose the motion of the tip, namely, only a part of the deformation energy translated into friction. This asymmetry is similar to the puckering[7] or viscoelastic ploughing.[26] Therefore, when μ_d was used to estimate the effect of deformation on friction, the physical meaning of λ should be the proportion of the asymmetry in the total deflection. Because it is very difficult to quantize the asymmetry of

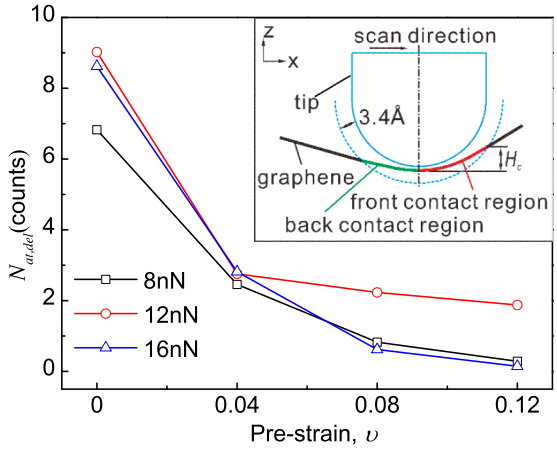

FIG. 5. Relationship between $N_{at,del}$ and the strain of graphene under various vertical loads. The inset is a schematic representation of contact region.

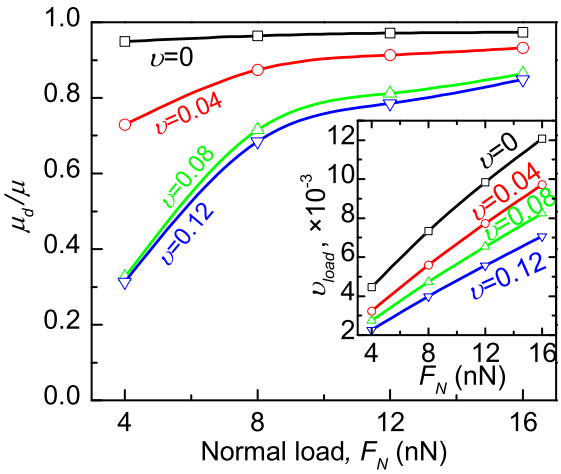

FIG. 6. Contribution of deformation in total friction. The inset shows the additional strain vs normal load curves.

the contact region, As presented in Fig. 5, we divided the contact region into two parts. The first one, in front of the tip center, can be called front contact region. The other one, behind of the tip center, can be called back contact region. The corresponding atom numbers of these two parts can be denoted as $N_{at,f}$ and $N_{at,b}$. The difference ($N_{at,del}$) between $N_{at,f}$ and $N_{at,b}$ was chosen to characterize the asymmetry of the contact region, i. e. $N_{at,del} = N_{at,f}$- $N_{at,b}$. As shown in Fig. 5, the curves experience abrupt drops with the increase of the pre-strain and tend to be stable gradually. This trend is very similar to friction coefficient.

According to the friction properties of suspended graphene,[25] out-of-plane deformation is the major factor contributing to friction. The ratio of μ_{vdw}/μ and μ_d/μ can be used to investigate the contribution of adhesion and deformation to total friction. As can be seen from Fig. 6, when υ=0, the contribution degree of deformation was over 90%. With the increase of pre-strain, the asymmetry of the contact region has been weakened ($N_{at,del}$ decreased rapidly) lead to a sharp decrease of the friction (Fig. 2). When the pre-strain reached 0.12, $N_{at,del}$ is close to zero, which implies the effect of asymmetry in the contact region can be ignored, Therefore, adhesion became the major factor of friction. But the pre-strain has little effect on adhesion (N_{at} decreased no more than 25% when υ changed from 0 to 0.12). Thus the descending rate of friction coefficient slowed down gradually with the increase of pre-strain.

Besides, the normal loads will lead to an additional strain. The effect of the additional strain is equal to that of the pre-strain. Additional strain in X-direction υ_{load} can be approximately calculated

by $\upsilon_{load} = ((1+\upsilon)^2 L_{x,\upsilon}^2 + \delta^2)^{1/2}/(1+\upsilon)L_{x,\upsilon} - 1$, where $L_{x,\upsilon}$ is one-half the length of graphene layer in x-direction under a pre-strain of υ. For non-pre-strained graphene (squares in inset in Fig. 6), the additional strain ranged from 0.4% to 1.2% when normal loads changed from 4 nN to 16 nN, which could result in a considerable decrease of the asymmetry (seen in Fig. 5) and finally reduce the friction coefficient. But for high pre-strained graphene (e.g. υ=0.12), we consider that the effect of additional strain can be ignored due to the fact that friction coefficient is not sensitive to strain in the case of high pre-strain and that υ_{load} is too small compared to pre-strain (<0.7%). However, this additional effect is not considered in Eq. (3) because λ is a constant under some certain strain. So the theoretical Eq. (3) is only suitable for the pre-strained graphene.

It is worth to note that no significant changes of $N_{at,del}$ can be observed under pre-strain situation when F_N is smaller than 4 nN. Because adhesive effect is the major factor of friction under in the condition of low loads and high pre-strain (down left of Fig. 6). So the asymmetry of the contact region is not obviously and could be over shadowed by thermal vibration.

B. Effect of the strain on the fluctuation of friction force

A periodic fluctuation of the friction force can be observed in all models. The averaged periodicity changing from 2.44 Å to 2.72 Å is in good correspondence with the theoretical lattice constant of graphene along ZZ direction that ranged from 2.46 Å to 2.76 Å with the increase of strain from 0 to 0.12. That can be explained by the periodic potential energy caused by periodic carbon atomic positions of the graphene.[24] Based on this theory, under a constant pre-strain, the tip-graphene distance decreases with increasing the vertical loads. On the other hand, contact stiffness increases with the increase of pre-strain. Therefore, the tip-graphene distance will also decrease with the increase of pre-stain. In both cases, the interaction between tip and graphene become stronger and the amplitude of the friction force (A_f) should increase. As shown in Fig. 7, heavy loads produced greater A_f when pre-strain is lower than 0.12 which is correspond to Ref. 24. But when pre-strain reached 0.12, A_f is approximately a constant. Furthermore, when heavy loaded ($F_N > 0$), A_f increased at first and following decreased with increasing the pre-strain, but when lightly loaded ($F_N = 0$), A_f decreased at first and then increased. These mentioned above are inconsistent with the results in Ref. 24. Dong et al[32] studied the effect of modified bending rigidity (approximately equal to contact sifness) on the friction of supported graphene by fixing atoms at their equilibrium crystalline positions. A similar trend that A_f decreased with increasing bending rigidity has been observed. But there is still some lack of fundamental understanding of this phenomenon.

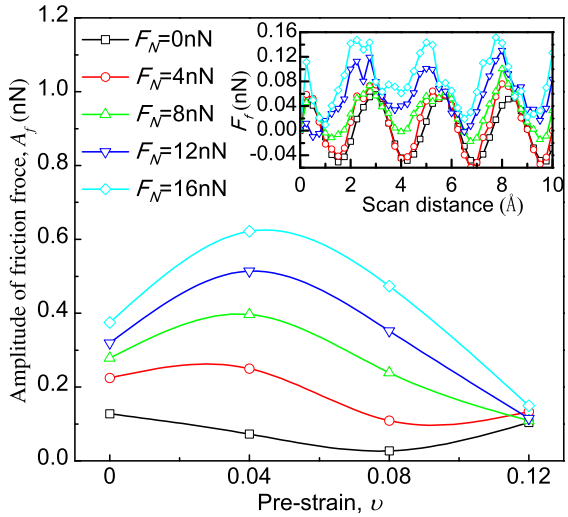

FIG. 7. Fluctuation of the friction force. The inset shows the variation of the friction force with the scan distance when pre-strain is 0.12.

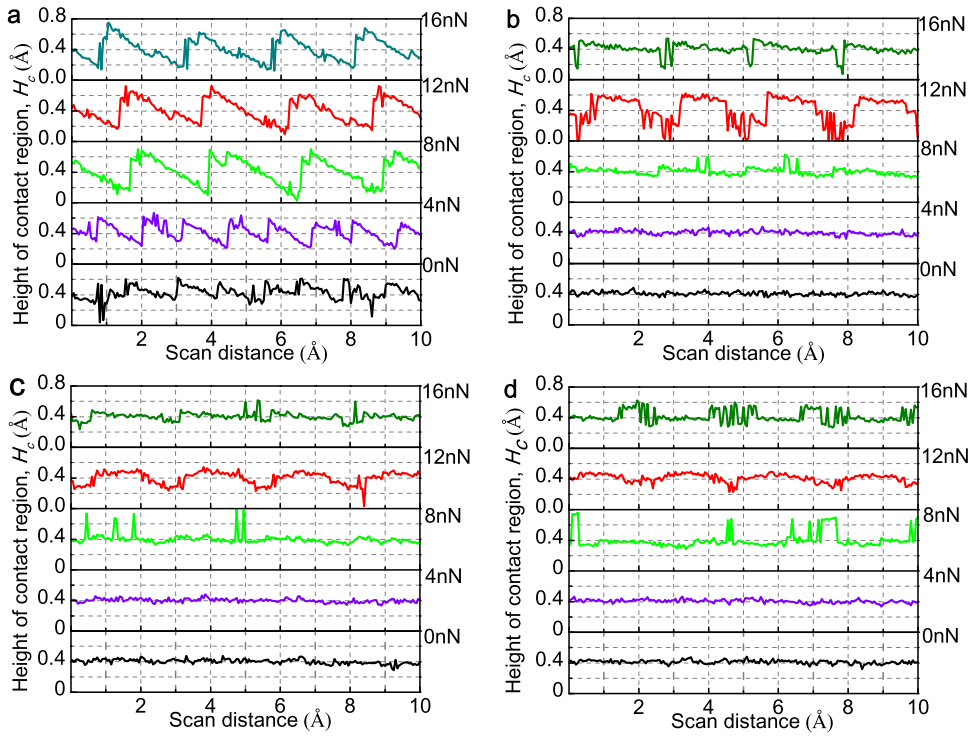

FIG. 8. Variation of the height of the contact region with the tip scan distance. The strain of a-d is 0, 0.04, 0.08, 0.12 respectively. For the sake of contractive analysis, each data set has been offset vertically.

Fig. 8 is the variation of the height of the contact region H_c (inset in Fig. 5) against the scan distance. H_c is also periodically fluctuant, and the periodicity of H_c is the same with that of the friction force. However, the specific fluctuation characteristics could be changed by pre-strain or normal load. The periodic interaction between the probe and the potential energy could lead to a fluctuation of the contact region which implies that the contact area (adhesive effect) and the deformation (ploughing effect) are both periodically fluctuant. Consequently, this fluctuation of the contact region can enhance the fluctuation of the friction force. The imposed pre-strain could increase the rigidity of graphene sheet, and thus can decrease the fluctuation of the contact region. Meanwhile, the additional strain (caused by loads) can also suppress the fluctuation of the contact region, especially when it is more considerable in low pre-strain condition. Otherwise, the interaction can be enhanced by normal loads and strain (both pre-strain and additional strain can decrease the contact area) which can increase the fluctuation of friction force. All of these intricate factors influence A_f together. The curves, resulting from the low-strained models (shown in Fig. 8(a), 8(b)), present a characteristic sawtooth appearance, which is very similar to the experimental friction force curves in Ref. 7 and can be regarded as the proof of the stick-slip event. In contrast, the curves obtained from the high pre-strained models (shown in Fig. 8(c), 8(d)) present a semi-arc appearance which indicates that the main interaction is mainly influenced by the periodic potential energy. It can also been found in Fig. 8 that the amplitude of H_c decreased grossly with the increase of the pre-stain in all models. And in the condition of low pre-strain (lower than 0.12), the amplitude of H_c increased firstly and following decreased with the increase of the normal load. However, it increased monotonously with the increase of normal load at the higher strain (strain =0.12). These trends are similar to the relationship between strain , normal loads and A_f (see Fig. 7).We further studied the relationship between H_c and A_f. The results shows that they are positively related when the graphene is pre-strained.

Finally, according to the analysis of the preceding context, it can be concluded that the periodic potential energy can lead to the periodic fluctuation of the contact region. The fluctuant properties of

the friction force are the composed action of these two factors. When the pre-strain is great enough, the fluctuation of friction force would be influenced by potential energy mainly.

IV. CONCLUSION

In the present work, the friction behavior between a strained suspended graphene and diamond tip has been simulated by MD simulation. The effect mechanism of strain on the frictional properties of suspend graphene has been revealed through the analysis of the contact state. It demonstrates that the asymmetry of the contact region is the main factor governing the friction of none-strained graphene. This asymmetry can be suppressed significantly by pre-strain, lead to one order of magnitude decrease of the friction coefficient, and thus, to the pre-strained graphene, the adhesive force becomes the major factor to friction. The fluctuation of the friction force is attributed to the composed effect of periodic potential energy and the fluctuation of the contact region. Pre-strain can also suppress the fluctuation of the contact region and improve the stability of friction process. These results could provide an atomic-level insight into the tribological behaviors of graphene or other atomically thin layers and promote the future application of strain-engineered graphene devices.

ACKNOWLEDGMENT

This research work was supported by the National Natural Science Foundation of China (Grant Numbers 51535003 and 51575138).

[1] Y. Zhang, Y. W. Tan, H. L. Stormer, and P. Kim, Nature **438**, 201 (2005).
[2] A. a. Balandin, S. Ghosh, W. Bao, I. Calizo, D. Teweldebrhan, F. Miao, and C. N. Lau, Nano Lett. **8**, 902 (2008).
[3] C. Lee, X. Wei, J. W. Kysar, and J. Hone, Science **321**, 385 (2008).
[4] M. Hirano and K. Shinjo, Phys. Rev. B **41**, 11837 (1990).
[5] M. Dienwiebel, G. S. Verhoeven, N. Pradeep, J. W. M. Frenken, J. a. Heimberg, and H. W. Zandbergen, Phys. Rev. Lett. **92**, 126101 (2004).
[6] Z. Liu, J. Yang, F. Grey, J. Z. Liu, Y. Liu, Y. Wang, Y. Yang, Y. Cheng, and Q. Zheng, Phys. Rev. Lett. **108**, 205503 (2012).
[7] C. Lee, Q. Li, W. Kalb, X. Z. Liu, H. Berger, R. W. Carpick, and J. Hone, Science **328**, 76 (2010).
[8] J. S. Choi, J.-S. Kim, I.-S. Byun, D. H. Lee, M. J. Lee, B. H. Park, C. Lee, D. Yoon, H. Cheong, K. H. Lee, Y.-W. Son, J. Y. Park, and M. Salmeron, Science **333**, 607 (2011).
[9] K. S. Novoselov, A. K. Geim, S. V Morozov, D. Jiang, Y. Zhang, S. V Dubonos, I. V Grigorieva, and A. A. Firsov, Science **306**, 666 (2004).
[10] A. K. Geim and K. S. Novoselov, Nat. Mater. **6**, 183 (2007).
[11] A. K. Geim, Science **324**, 1530 (2009).
[12] Q. Li, C. Lee, R. W. Carpick, and J. Hone, Phys. Status Solidi Basic Res. **247**, 2909 (2010).
[13] Y. Dong, J. Phys. D. Appl. Phys. **47**, 055305 (2014).
[14] D.-H. Cho, L. Wang, J.-S. Kim, G.-H. Lee, E. S. Kim, S. Y. S. Lee, S. Y. S. Lee, J. Hone, and C. Lee, Nanoscale **5**, 3063 (2013).
[15] Z. Deng, A. Smolyanitsky, Q. Li, X.-Q. Feng, and R. J. Cannara, Nat. Mater. **11**, 1032 (2012).
[16] T. Filleter, J. L. McChesney, A. Bostwick, E. Rotenberg, K. V. Emtsev, T. Seyller, K. Horn, and R. Bennewitz, Phys. Rev. Lett. **102**, 1 (2009).
[17] T. Filleter and R. Bennewitz, Phys. Rev. B **81**, 155412 (2010).
[18] M. Reguzzoni, A. Fasolino, E. Molinari, and M. C. Righi, J. Phys. Chem. C **116**, 21104 (2012).
[19] L. Xu, T.-B. Ma, Y.-Z. Hu, and H. Wang, Nanotechnology **22**, 285708 (2011).
[20] S. Kwon, J.-H. Ko, K.-J. Jeon, Y.-H. Kim, and J. Y. Park, Nano Lett. **12**, 6043 (2012).
[21] J.-H. Ko, S. Kwon, I.-S. Byun, J. S. Choi, B. H. Park, Y.-H. Kim, and J. Y. Park, Tribol. Lett. **50**, 137 (2013).
[22] A. L. Kitt, Z. Qi, S. Rémi, H. S. Park, A. K. Swan, and B. B. Goldberg, Nano Lett. **13**, 2605 (2013).
[23] Z. Deng, N. N. Klimov, S. D. Solares, T. Li, H. Xu, and R. J. Cannara, Langmuir **29**, 235 (2013).
[24] P. Liu and Y. W. Zhang, Carbon **49**, 3687 (2011).
[25] A. Smolyanitsky, J. P. Killgore, and V. K. Tewary, Phys. Rev. B **85**, 035412 (2012).
[26] A. Smolyanitsky and J. Killgore, Phys. Rev. B **86**, 125432 (2012).
[27] T. Schneider, E. P. Stoll, and R. Morf, Phys. Rev. B **18**, 1417 (1978).
[28] S. Stuart, A. Tutein, and J. Harrison, J. Chem. Phys. **112**, 6472 (2000).
[29] Y. J. Shin, R. Stromberg, R. Nay, H. Huang, A. T. S. Wee, H. Yang, and C. S. Bhatia, Carbon **49**, 4070 (2011).
[30] Y. Mo, K. T. Turner, and I. Szlufarska, Nature **457**, 1116 (2009).
[31] M. Dienwiebel, N. Pradeep, G. S. Verhoeven, H. W. Zandbergen, and J. W. M. Frenken, Surf. Sci. **576**, 197 (2005).
[32] Y. Dong, X. Wu, and A. Martini, Nanotechnology **24**, 375701 (2013).